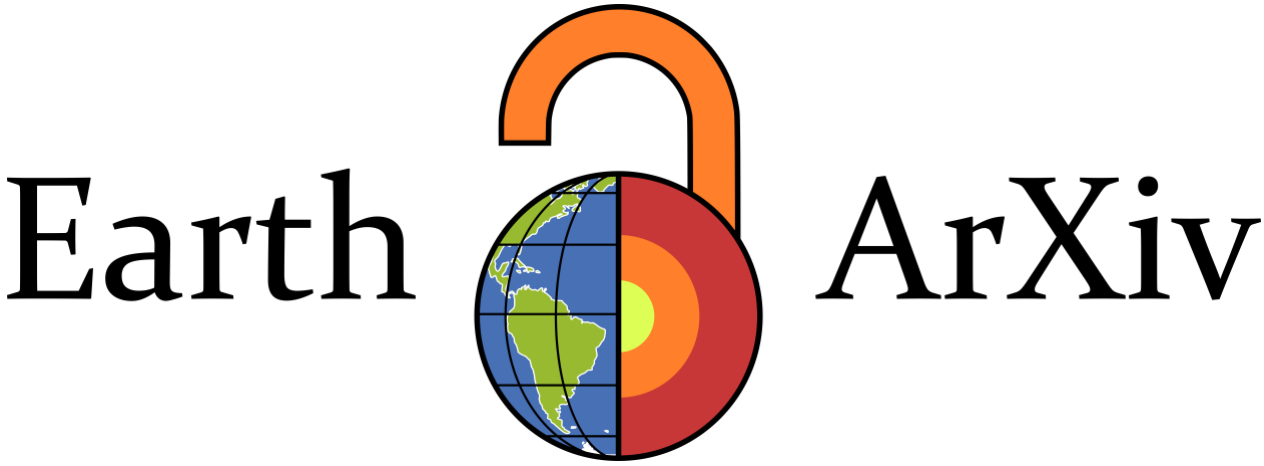

A BIAS-CORRECTED & DOWNSCALED MASSIVE ENSEMBLE TO DIAGNOSE UNCERTAINTY IN CLIMATE IMPACT PROJECTIONS

Kevin Schwarzwald[1,2], Nathan Lenssen[3,4], Radley M. Horton[1,2], and Gernot Wagner[5]

[1]Columbia Climate School, New York, NY, USA
[2]Lamont-Doherty Earth Observatory of Columbia University, Palisades, NY, USA
[3]Colorado School of Mines, Golden, CO, USA
[4]NSF National Center for Atmospheric Research, Boulder, CO, USA
[5]Columbia Business School, New York, NY, USA

February 23, 2026

ABSTRACT

Projections of climate change and climate impacts requires bias-corrected, downscaled output from ensembles of earth system models (ESMs). Potential impacts are uncertain due to modeling differences between ESMs, internal variability stemming from the chaos of the earth system, and differences in the historical reference datasets used to bias-corrected and downscale ESM output. Here, we introduce the Bias-Corrected and Downscaled Massive Ensemble (BCD-ME), a set of over 1,400 projections of daily mean and maximum temperature. The BCD-ME samples model and internal uncertainty with up to 86 runs from 12 Large Ensembles and uncertainty in the reference dataset by using 4 different reanalysis products to bias-correct and downscale output. Output is organized by Global Warming Levels (GWL), accounting for differences between forcing scenarios and ESM climate sensitivities. The ensemble contains 20-year daily time series for each GWL on a uniform 1° grid, bias-corrected using Quantile Delta Mapping, and statistics of 20-year time series for each GWL on a uniform 0.25° grid, downscaled using Quantile-Preserving Localized Analog Downscaling. The BCD-ME is stored in Analysis-Ready, Cloud-Optimized (ARCO) Zarr stores, enabling efficient computation of the 97 TB (uncompressed) dataset.

1 Background & Summary

Climate impact assessments help predict changes in human and natural systems due to climate change. Generally, these studies seek to find a statistical or process-based relationship between the climate and an impact over some observed, historical period and then use this relationship to predict changes in the impact given some change to the climate. Estimates of future climates are critical in this process, generally referred to as "climate projections". Climate projections are most commonly derived from simulations made with dynamical Earth System Models (ESMs) as part of the Coupled Model Intercomparison Project (CMIP, Eyring et al. (2016)).

There are three major knowledge barriers to properly using CMIP-class ESMs' climate projections in climate impacts studies. First, uncertainty in future climate must be included and properly propagated to the estimate of future impacts, stemming from differences between forcing scenarios, differences between ESMs, and the internal variability due to the chaotic nature of the earth system (Tebaldi and Knutti, 2007; Hawkins and Sutton, 2009; Auffhammer et al., 2013; Rising et al., 2022; Schwarzwald and Lenssen, 2022). The climate impacts community is increasingly accounting for climate uncertainty due to possible future scenarios and differences in climate models (Burke et al., 2015). Including uncertainty due to internal climate variability has been shown to be important as well, but has lagged, since proper treatment of internal uncertainty requires applying analyses to hundreds of climate model projections (Schwarzwald and Lenssen, 2022).

Second, raw values from ESM output are biased relative to the true Earth's climate in both the mean and higher moments of key climate variables. While ESMs simulate the climate with underlying physics, chemistry, and biology as currently understood, due to modeling limitations they do not exactly replicate the observed climate, and are run with no requirement that the output has equal statistics to the true Earth system (Maraun, 2016; Auffhammer et al., 2013); ESM output must, thus, be bias-corrected before it can be used in impacts contexts (Auffhammer et al., 2013).

Finally, CMIP-class ESMs generally utilize atmospheric models with spatial resolutions of $0.7 - 2.8°$ (approx. 100-300 km at the equator) and are therefore unable to provide local estimates of key variables at impact-relevant spatial scales, particularly in regions with complex geography Schulze (2000); Hsiang et al. (2017); ESM output is, thus, often downscaled before use in impacts contexts.

Bias-correction and statistical downscaling methods require a spatially and temporally complete product of observed climate. Climate reanalyses or other gridded historical data products are typically used for this purpose as direct weather observations have gaps in spatial and temporal coverage, particularly prior to the satellite era. However, reanalyses provide imperfect estimates of climate variables with uncertainty arising due to limitations in the dynamical model, the assimilation scheme, and uncertainty in the data assimilated into the reanalysis, adding an additional source of uncertainty in climate projections.

To properly overcome all three of these knowledge barriers, a research group must therefore have sufficient computational resources and technical expertise to download and store hundreds of climate model projections, implement or develop bias-correction and downscaling methods, and apply these to each climate projection. Together, these steps are a massive investment in computing, disk storage, and software development that all ought to be supported by expertise from climate and statistical experts. The scale of this investment is a major barrier to entry into studying climate impacts. Existing publicly-available products aimed at impacts research, such as NASA Earth Exchange Global Daily Downscaled Projections (NEX-GDDP, Thrasher et al. (2022)), the Inter-Sectoral Impact Model Intercomparison Project (ISIMIP, Frieler et al. (2024), or the Global Downscaled Projections for Climate Impact Research (GDPCIR, Gergel et al. (2024)) provide bias-corrected and downscaled climate projections, but do not sample internal variability (only one ensemble member per ESM is provided). A notable exception are the recent GARD-LENS (Hartke et al., 2024) and LOCA2 (Pierce et al., 2023) products, which provide output from several large ensembles at very high resolution; however, these products are limited to North America. Furthermore, none of these products samples the uncertainty in datasets used to post-process ESM output (only one reanalysis or other gridded historical reference dataset is used in each product).

1.1 Summary of the BCD-ME

To fill this gap, in this data descriptor we present the Bias-Corrected & Downscaled Massive Ensemble (BCD-ME), a near-surface air temperature projection dataset designed to make it as straightforward as possible to include climate uncertainty in analyses. The BCD-ME addresses the knowledge barriers discussed above, including uncertainty due to the reanalysis product used. The key features of this dataset include:

- **Daily average and maximum temperature with near-global land coverage** to enable global and regional analyses of temperature projections and climate impact projections.
- **Indexed by global warming levels (GWLs)** to facilitate direct comparisons of ESMs with different climate sensitivities.
- **Bias-Corrected** time series on a uniform $1°$ grid using Quantile Delta Mapping (QDM) (Cannon et al., 2015).
- **Downscaled** statistics of bias-corrected time series on a $0.25°$ grid using Quantile-Preserving Localized Analog Downscaling (QPLAD) (Gergel et al., 2024).
- **Sampling climate model uncertainty** using 12 different ESMs
- **Sampling internal variability** using between 5 and 86 ensemble members from each ESM.
- **Sampling "ground-truth" uncertainty** using 4 reanalyses of historical climate to bias-correct and downscale ESM output.
- **Provided in Zarr stores** and on the cloud for efficient computation.

We use four products as possible observational ground truths in the bias-correction and downscaling. (1) The European Centre for Medium-Range Weather Forecasting Reanalysis v5 (ERA5) Hersbach et al. (2020) (2) The NASA Modern-Era Retrospective analysis for Research and Applications, Version 2 (MERRA2) (Gelaro et al., 2017) (3) The Japanese Meteorological Agency Japanese Reanalysis for Three Quarters of a Century (JRA-3Q) (Kosaka et al., 2024) (4) The Global Meteorological Forcing Dataset (GMFD) (Sheffield et al., 2006). The first three are state-of-the-art operational

Reanalysis	Resolution	Publisher	Citation
ERA5	0.25°	European Centre for Medium-Range Weather Forecasting (ECMWF)	(Hersbach et al., 2020)
MERRA2	0.5° x 0.625°	National Aeronautics and Space Administration (NASA)	(Bosilovich et al., 2015)
JRA-3Q	0.375°	Japan Meteorological Agency (JMA)	(Kosaka et al., 2024)
GMFD	0.25 °	Princeton Hydrology Group	(Sheffield et al., 2006)

Table 1: Reanalysis products used as historical "ground truths" for bias-correction and downscaling

reanalyses. GMFD is included as it is used to bias-correct the NASA NEX-GDDP (Thrasher et al., 2022) and is therefore commonly used in climate impact research (Carleton et al., 2022; Hultgren et al., 2025; Rode et al., 2021).

The BCD-ME contains two collections of data: (1) bias-corrected time series on a uniform $1^\circ \times 1^\circ$ grid and (2) selected metrics commonly used in climate impacts studies on a uniform $0.25^\circ \times 0.25^\circ$ (see Table 3 for descriptions). We provide statistics on the downscaled 0.25° grid, rather than the full daily time series, to increase the usability of this very large dataset. The BCD-ME time series collection provides bias-corrected time series 2m daily temperature (`tas`) and 2m maximum daily temperature (`tasmax`) for all locations from 56°S to 86°N (land-only for GMFD-based ensemble members), spanning all permanently inhabited regions. The 0.25° downscaled product provides bias-corrected and downscaled metrics for all land locations over the same spatial extent.

The presented BCD-ME dataset contains on the order of 100 times more impact assessment-ready temperature projections than the commonly used NASA NEX-GDDP dataset (Thrasher et al., 2022). The organization of the BCD-ME enables users to easily account for all sources of climate uncertainty by indexing across uncertainty-relevant dimensions. The computational costs of scaling an impacts analysis by a factor of 100 is reduced by providing the BCD-ME as I/O-optimized Zarr stores that enable code bases to be easily scaled and parallelized on modest systems.

In the remainder of this paper, we outline the source data and methods used to construct the BCD-ME, provide a validation of the dataset, and provide suggestions for best practices when working with this data. We expect that the BCD-ME will be useful for users of climate projection information by enabling the robust quantification of uncertainty in future climate.

2 Methods

There are four major components in the creation of the BCD-ME (see summary diagram in Figure 1). Section 2.1 details the ESM and reanalysis data used as the raw inputs to the BCD-ME. Section 2.2 discusses how GWLs are calculated for each climate projection, how the data is organized by these GWLs, and presents analysis justifying the use of GWLs. Section 2.3 details the bias-correction methods and Section 2.4 details the downscaling method.

2.1 Input Data

2.1.1 CMIP6 Large Ensemble MIP

We aim to use all simulations from the CMIP6 Large Ensemble MIP available on Pangeo's CMIP6 cloud storage (`https://console.cloud.google.com/marketplace/product/noaa-public/cmip6`) that have daily output for daily mean (`tas`) or max (`tasmax`) near-surface air temperature for a historical experiment starting at the latest on January 1, 1850, and a future ScenarioMIP experiment forced with any Shared Socioeconomic Pathway (SSP) (Riahi et al., 2017), resulting in 12 ESMs with ensemble sizes ranging from 8 to 86. Currently, this includes 365 total members for `tas` and 190 for `tasmax`, with future versions of the dataset including more members as they are processed or become available on pangeo. These ensemble sizes include all projections run with the model, across all SSPs. A full description of the ESMs used is shown in Table 4. Note that ESM output is regridded bilinearily to a uniform 1-degree latitude/longitude grid before bias-correction (Step **1** in Figure 1).

2.1.2 Global Reanalysis

Bias-correction and downscaling both rely on knowing the Earth's true climate over some observed time period. However, there is non-negligible uncertainty in estimates of the true historical climate (Morice et al., 2021; Lenssen et al., 2024). Despite this uncertainty, climate impact studies generally use a single reanalysis product, failing to sample both uncertainty in the raw data assimilated into the reanalysis as well as structural uncertainties in the underlying dynamical model. In the BCD-ME, we sample this reanalysis uncertainty by repeating the bias-correction and downscaling with four reanalyses (see Table 1): the European Centre for Medium-Range Weather Forecasting ERA5 (Hersbach et al., 2020), NASA MERRA2 (Bosilovich et al., 2015), the Japan Meteorological Agency JRA-3Q (Kosaka et al.,

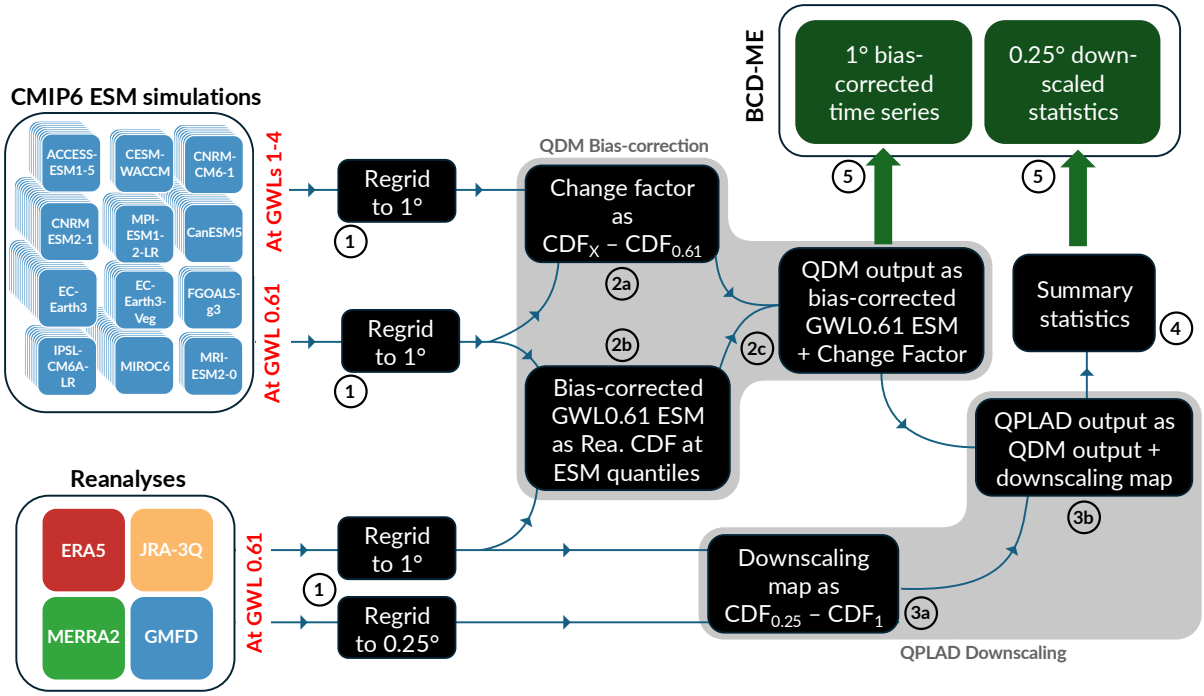

Figure 1: Diagram of bias-correcting and downscaling workflow. Reanalysis data for the 20 years around GWL0.61 (1982-2001) is regridded to uniform 1° and 0.25° grids; data from ESM runs for the 20 years around GWLs 0.61 and 0.5°C steps from GWL1 to 4 (or the highest GWL step reached) are regridded to a uniform 1° grid (Step **1**). Processing is done separately for each combination of an ESM run and a reanalysis 'ground truth'. 1-degree ESM and reanalysis data is used to create bias-corrected time series through the QDM methodology (Step **2**). That bias-corrected output is combined with a downscaling map from reanalysis between 1° and 0.25° to create downscaled time series through the QPLAD methodology (Step **3**). Finally, summary statistics (detailed in Table 3) of the 0.25°-degree time series are calculated (Step **4**). For each ESM run and reanalysis, one set of bias-corrected time series on a 1° grid and one set of statistics of the bias-corrected and downscaled time series on a 0.25° grid are thus saved, forming the BCD-ME (Step **5**).

2024), and GMFD (Sheffield et al., 2006). ERA5, MERRA2, and JRA-3Q are latest-generation, continuously updating global reanalysis products, while GMFD is used as the "ground truth" for NASA's NEX GDDP (Thrasher et al., 2022) set of bias-corrected and downscaled climate projections and is therefore frequently used as a source of historical weather observations in projections of climate impacts (Carleton et al., 2022; Rode et al., 2021; Hultgren et al., 2025). While this is not a complete assessment of uncertainty in the observed climate, there are substantial differences between these four products, providing the ability to determine the sensitivity of climate impact projections to the choice of ground-truth observations.

Reanalysis products are used at two resolutions (Step **1** in Figure 1). For bias-correction, output from reanalyses is bilinearly regridded to a uniform 1-degree latitude/longitude grid. For downscaling, output from reanalyses is bilinearly regridded to a uniform 0.25-degree latitude/longitude grid that exactly nests into the 1-degree grid such that each 1-degree grid cell contains 4 0.25-degree grid cells.

Note that 0.25 degree is a finer resolution than two of the reanalyses used (MERRA2 and JRA-3Q). Thus, the 0.25 degree projections from MERRA2 and JRA-3Q cannot contain information finer than the native grids of these reanalyses (See Table 1) and are constructed by interpolation from these native reanalysis grids. Nevertheless, we provide all four downscaled products at the 0.25 degree grid to facilitate comparison. Users should use caution when interpreting fine-scale spatial features in MERRA2 and JRA-3Q 0.25 degree projections.

2.2 Global Warming Levels

Rather than providing projections as continuous time series over the 21st century, we instead organize the BCD-ME by 20-year daily time series at given Global Warming Levels (GWLs). GWLs are degrees of global mean near-surface

air temperature warming relative to the 1850-1900 baseline (Seneviratne and Hauser, 2020). For instance, the '2°C world' envisioned by the Paris Agreement considers climate conditions and impacts at GWL2.

Future climate impacts are increasingly presented by GWL including in the sixth IPCC assessment report, due to several key advantages over time-series-based projections. First, data presented at GWLs is agnostic to climate sensitivity, helping avoid the so called "hot model" problem from ESMs with possibly unrealistically high climate sensitivities in CMIP6 (Hausfather et al., 2022). Note that this removes intermodel differences in global climate sensitivity as a driver of model uncertainty; the intermodel spread will therefore be reduced compared to an analysis at a comparative set of calendar years.

Second, data presented at GWLs control for differences between climate scenarios, such as the Shared Socioeconomic Pathways (SSPs) (Riahi et al., 2017) used in the CMIP6 ScenarioMIP set of experiments. These SSPs are socioeconomic storylines of future anthropogenic forcings, such as greenhouse gas and aerosol concentrations or land use patterns, and are not intended to provide a statistical sampling of plausible future conditions. Abstracting away from differences in warming rates between SSPs allows a user to assume their own preferred timeline of warming (including by examining scenarios such as the Paris Agreement or using GMSTs estimated from integrated assessment models).

Third, by pooling ensemble members from different SSPs at the same GWL, users of climate data are able to boost the ensemble size for each ESM. These larger ensemble sizes enable characterization of ESM internal variability for a larger set of ESMs(Milinski et al., 2020).

2.2.1 GWL Identification and Data Organization

In the BCD-ME, we utilize a global warming level index `GWL` rather than indexing by a calendar year in the future, providing 20 years of daily simulations at 8 GWLs: 0.61, 1.0, 1.5, 2.0, 2.5, 3.0, 3.5, and 4.0 °C. The 0.61 °C equals the observed global mean temperature over the 20 year period of 1982-2001 in HadCRUT5 (Morice et al., 2021) and was used as a reference time to bias-correct and downscale ESM output, and together with GWL1 (2001-2020 in HadCRUT5) may be useful for climate impact studies that investigate the changes in climate risk compared to a period close to present.

A GWL is defined by the global mean temperature anomaly relative to a 1850-1900 baseline following the IPCC definition for warming compared to the preindustrial. For each climate model ensemble member, we calculate the global mean surface annual temperature anomaly and compute a 20 year moving average. Then, for each GWL, we find the first year that this moving average crosses the given GWL, and define the 20 years around this year as the climate for this GWL (Seneviratne and Hauser, 2020; Batibeniz et al., 2023).

For a given GWL, 20 years of daily temperature fields are then provided in the BCD-ME, indexed by `year` from `1:20` and `dayofyear` from `1:365`. As an example, in the r1i1p1f1 member of the MPI-ESM1-LR model run under SSP2.45, the 20-year rolling average of global mean temperature is more than 1 degree above its 1850-1900 mean for the first time in 2013. Thus, we define the 20-year time period of 2003-2022 as an ensemble member for this model for the 1.0 °C GWL. We additionally provide the calendar years from the ESM simulation as the auxiliary dimension `calendar_year`, but recommend users utilize the GWL setup of the data whenever possible. Note that many model projections will not reach every GWL, with only the warmest models under high emissions scenarios reaching the 4.0 °C GWL. The number of simulations available at each GWL for each model is presented in Table 2.

2.3 Bias-Correction: Quantile Delta Mapping

Since the probability distributions of climate variables in an ESM differ from those in the true Earth, ESM output is generally bias-corrected in climate impacts context to make values directly usable in climate impact models trained on historical observations.

Here, we use the Quantile Delta Mapping (QDM) (Cannon et al., 2015) method (Step **2** in Figure 1). QDM uses a "delta method" approach, adding changes between present and future time periods from an ESM to a time series taken from a reference data product. QDM allows for different change factors for each quantile of an ESM's distribution. That change factor is then added to the reference data sampled at the quantiles of the ESM's time series, equivalently referred to as a bias-corrected version of the historical ESM data (Cannon et al., 2015).

Each day-of-year is processed separately using a moving window of 31 days for each day-of-year to calculate CDFs. At a given location and each day of year, the changes between the empirical CDF of the ESM run at a reference GWL (0.61, representing 1982-2001 in the real world) and the empirical CDF of a future GWL is found, using 100 samples of quantiles to estimate the CDF (Step **2a**). Then, for each day in the future period, the same quantile is found in the reference reanalysis dataset (Step **2b**), and the difference in the CDF at that quantile and day of year of the GWL is added to it (Step **2c**). The difference between the future ESM and GWL 0.61 ESM CDFs thus provides the necessary

Variable	GWL reached: Model	1.0	1.5	2.0	2.5	3.0	3.5	4.0
tas	ACCESS-ESM1-5	24	24	24	24	5	5	5
	CESM2-WACCM	8	8	8	7	7	4	3
	CNRM-CM6-1	18	18	18	18	15	12	6
	CNRM-ESM2-1	41	41	31	26	13	7	5
	CanESM5	86	86	86	86	86	86	79
	EC-Earth3	35	35	35	35	32	15	10
	EC-Earth3-Veg	13	13	13	13	13	9	6
	FGOALS-g3	10	10	10	7	3	0	0
	IPSL-CM6A-LR	28	28	28	28	28	18	17
	MIROC6	60	34	34	31	28	0	0
	MPI-ESM1-2-LR	30	30	30	20	16	6	0
	MRI-ESM2-0	12	8	8	8	7	2	0
	Total	365	335	325	303	253	164	131
tasmax	ACCESS-ESM1-5	6	6	6	6	6	6	6
	CESM2-WACCM	0	0	0	0	0	0	0
	CNRM-CM6-1	5	5	5	3	2	2	1
	CNRM-ESM2-1	5	5	3	3	2	1	1
	CanESM5	30	30	30	30	30	30	27
	EC-Earth3	22	22	22	22	19	8	3
	EC-Earth3-Veg	10	10	10	10	10	5	2
	FGOALS-g3	7	7	7	4	0	0	0
	IPSL-CM6A-LR	22	22	22	22	22	12	11
	MIROC6	37	25	25	22	19	0	0
	MPI-ESM1-2-LR	30	30	30	20	16	6	0
	MRI-ESM2-0	16	16	16	14	11	6	0
	Total	190	178	176	156	137	76	51

Table 2: Number of runs in the BCD-ME that (as of version 1) have data for at least a given GWL, by ESM, for near-surface mean daily air temperature (`tas`, top half) and near-surface maximum daily air temperature (`tasmax`, bottom half).

correction factor of the reanalysis data. That is, for $x_m(t)$, a ESM projection m at time t in the future, we calculate the adjusted $x^*_m(t)$ as:

$$x^*_m(t) = x_m(t) + \left(F_o^{-1}(q) - F_m^{-1}(q)\right) \tag{1}$$

where F_o^{-1} and F_m^{-1} are the empirical inverse CDFs of the observed historical climate and the ESM climate respectively. Finally, q is the quantile associated with the value of $x_m(t)$ in the ESM's simulation. We roughly follow the notation in Section 3.1 of Gergel et al. (2024) which contains more background on this method.

As an example, if the 0.6 quantile of a ESM simulation at a location at GWL1 is 14.5 °C and the 0.6 quantile of the same ESM run at this same location at GWL0.61 is 13.8 °C, the 0.6 quantile from the reanalysis for this day of year is projected by adding 0.7 °C.

2.4 Downscaling: Quantile-Preserving Localized-Analog Downscaling

The Large Ensemble ESMs simulation used here for temperature projections have native grids ranging in resolution from 0.7° to 2.8° (approx. 100-300 km at the equator). There is need in the climate impact community for information at as fine a spatial scale as possible, motivating the downscaling of these products. Here, we implement Quantile-Preserving Localized-Analog Downscaling (QPLAD) for statistically downscaling the ESM output to a finer resolution reanalysis grid, following Gergel et al. (2024) (Step **3** in Figure 1).

Similar to the QDM bias-correction, QPLAD is a non-parametric quantile-based method that provides estimates of the temperature at the fine-scale. First, a downscaling map is created using the reference reanalysis datasets (Step **3a** in Figure 1). We use the 1982-2001 reanalysis data regridded to a 1-degree grid from above, and also bilinearily regrid the reanalysis data to a uniform 0.25-degree grid that perfectly slots into the 1-degree grid such that each low-resolution grid cell exactly contains 4 high-resolution grid cells. For each reanalysis, the downscaling map is the difference in empirical CDFs (using all empirical quantiles) between the 1-degree data and the 0.25-degree data. As before, separate

Metric	Units	Description	Notes
Bias-corrected variables (1° grid)			
`tas`	K	Near-surface mean daily temperature	Time series
`tasmax`	K	Near-surface maximum daily temperature	Time series
Bias-corrected and downscaled metrics (0.25° grid)			
`tasbinC`	days / year	Mean days per year in Celsius bins	1-deg bins from -21.5 to 51.5°C
`tasbinF`	days / year	Mean days per year in Fahrenheit bins	5-deg bins from -5 to 130 F
`tassumpoly`	$°C^k$ for $k \in (1, 2, 3, 4)$	Mean annual sums of polynomial mean temperature	
`tasmaxbinC`	days / year	Mean days per year in Celsius bins	1-deg bins from -21.5 to 51.5°C
`tasmaxbinF`	days / year	Mean days per year in Fahrenheit bins	5-deg bins from -5 to 130 F
`tasmaxsumpoly`	$°C^k$ for $k \in (1, 2, 3, 4)$	Mean annual sums of polynomial max temperature	

Table 3: Description of saved variables in the 1° bias-corrected and 0.25° bias-corrected and downscaled BCD-ME products.

CDFs are calculated for each day-of-year, using a 31-day rolling window across each of the 20 years centered at that day-of-year, resulting in 620 (31 x 20) empirical quantiles.

Then, for each day at every location and GWL in each 1-degree bias-corrected ESM simulation, the downscaling map at the relevant day-of-year and quantile (as before, calculated relative to a 31-day-of-year moving window across years) is added to its value to produce values at each of the 4 nested 0.25-degree grid cells within (Step **3b** in Figure 1). See Gergel et al. (2024) for more details.

We note that, of the four reanalysis datasets used as downscaling "ground truths", JRA-3Q (0.375°) and MERRA2 (0.5° x 0.675°) are of lower resolution than the 0.25-degree resolution of the downscaled datasets. We use them to downscale to the same uniform 0.25-degree grid as reference, but note that values of the downscaling map at a higher resolution than their native resolution are statistically interpolated and do not provide more information from the model. Users should therefore treat those values with caution.

2.4.1 Downscaled metrics

Due to the size of the dataset, we do not provide full time series at the 0.25-degree resolution of the downscaled data. Rather, we save summary statistics commonly-used in climate impacts work, averaged across the 20 years for each GWL (Step **4** in Figure 1; see Table 3 for details).

For both mean and maximum daily temperature, we save the number of days in 1 °C and 5 °F bins (`tasbinC`, `tasbinF`, `tasmaxbinC`, and `tasmaxbinF`). These are commonly used in binned non-parametric statistical impact models and to study threshold exceedance following Schlenker and Roberts (2009) and Deschênes and Greenstone (2011). We also provide summed polynomials up to degree 4, allowing for flexible nonlinear dose-response functions (see, e.g., Carleton et al. (2022)), as `tassumpoly` and `tasmaxsumpoly`:

$$sumpoly = \sum_{d=1}^{365} T^k \text{ for } k \in \{1, 2, 3, 4\}$$

In other words, k = 2 shows the sum of squared temperature.

3 Data Records

The BCD-ME is presented as an ensemble with multiple ESMs and multiple ensemble members from each of the ESMs. Rather than providing the full daily time series over the projection period of 2015-2100, we instead provide 20-year daily time series (for the 1-degree bias-corrected set) and statistics of 20-year daily time series (for the downscaled 0.25-degree set) from each ESM such that the ESM ensemble mean has a specific global mean temperature value or global warming level (GWL). There has been a recent shift to using GWLs instead of time periods in climate projection-related studies, primarily due to the fact that the CMIP6 generation contains models with climate sensitivities outside the range deemed to be plausible or the so-called "hot model" problem (Hausfather et al., 2022)). Thus, we provide 20-year series at 0.61 °C (equivalent to the mean observed global temperature from 1982-2001 in HadCRUT5 (Morice et al., 2021)) of warming relative to 1850-1900 (historical) as well as GWLs of 1.0-4.0 °C in 0.5 °C increments. Thus, including the four different reanalyses used in bias-correction and the GWLs, the dataset can be

viewed as a 7-dimensional array

$$\texttt{BCD-ME}[\texttt{lon}, \texttt{lat}, \texttt{time}, \texttt{GWL}, \texttt{reanalysis}, \texttt{ESM}, \texttt{experiment/ensemble\_member}] \tag{2}$$

for the 1-degree time series and

$$\texttt{BCD-ME}[\texttt{lon}, \texttt{lat}, \texttt{D}, \texttt{GWL}, \texttt{reanalysis}, \texttt{ESM}, \texttt{experiment/ensemble\_member}] \tag{3}$$

for the 0.25-degree statistics, with the dimension D being unique to each particular variable (e.g., temperature bin).

To facilitate computation with this massive array, all of the data has been archived in the `Zarr` format, with a separate `Zarr` store for each ESM and data type. For example, for the ESM ACCESS-ESM1-5, one `Zarr` store contains all 1° bias-corrected time series in variables `tas` and `tasmax`, and one `Zarr` store contains all 0.25° downscaled statistics from both `tas`-based and `tasmax`-based variables. We recommend working with the data in Python with the `Xarray` and `Dask` libraries as these packages make parallelized I/O and computation relatively simple and efficient to implement (Abernathey et al., 2021).

The Zarr stores are chunked to facilitate regional analyses. In other words, a chunk will contain all days (for bias-corrected time series) or all bins or polynomial degrees (for downscaled statistics) for a sub-continental-scale region for one ensemble member, GWL, and reanalysis.

Since not every ensemble member reaches every GWL, and not every ensemble member has data for each variable, each Zarr store contains a metadata coordinate `has_data`, a `variable x ensemble member x GWL` boolean array detailing which elements have data.

The full BCD-ME data is stored and hosted as `Zarr` stores in two repositories: one that will be frozen upon the publication of this article and one that will be updated. The dataset (in its form upon acceptance of this manuscript) will be archived in the National Science Foundation (NSF) National Center for Atmospheric Research (NCAR)'s Geoscience Data Exchange (GEX). The NSF NCAR GEX provides open access to data through HTTPS and Globus, promotes FAIR principles including issuing a DOI, and enables users to work quickly with the data on the NCAR computer systems.

The BCD-ME is also freely available via the Earthmover Data Marketplace in an Analysis-Ready, Cloud-Optimized format (Abernathey et al., 2021). This version of the BCD-ME is a "cloud-native data repository" (Abernathey et al., 2021) that allows fast and efficient processing despite its size, with access occurring natively within `xarray`. Links to sample code to access this data is provided in the Data Availability section below. The version of this dataset will not be frozen, but any updates to the data will be fully tracked through version control, similar to how code revisions are documented through git repositories. Users accessing this repository will have the latest version of this data and improved I/O due to the optimizations of handling array data provided by Icechunk.

4 Technical Validation

4.1 GWL Assumptions and Validation

The primary assumption underlying presenting results by GWL is that local climate conditions are dependent only on the amount of warming (represented by GMST) rather than the pathway of warming taken up to that point. Two notable ways in which this could affect results across the ScenarioMIP archive is through the speed of warming–for instance, the Earth is projected to reach 2.0 °C GWL in 2046 under SSP 2-4.5, but an earlier 2038 under the higher emission SSP 5-8.5 (in the BCD-ME, 2036-2055 from the former simulation and 2028-2047 from the latter are presented as equivariant simulations at GWL2)–and the dependence on the exact mix of greenhouse gases, aerosols, and other forcings, which may be different at a certain GWL between SSPs.

To confirm that our use of GWL is justified, we show that GWLs are a very good predictor of regional climate distributions. The distributions in the difference between GWL 2 and the historical GWL 0.61 at the regional level are indistinguishable between SSPs with no notable bias in mean, variance, or other moments for a particular SSP (Figure 2). Even SSP3-7.0, which represents a different aerosol trajectory than the other SSPs (Shiogama et al., 2023), shows a similar distribution of temperature at each GWL to the other scenarios. This analysis was repeated with other GWLs, with similar results.

4.2 Physicality of Temperature

As a first-pass validation of the final BCD-ME data products, we check for unexpected missing values and confirm that all temperatures are physically possible. For downscaled statistics, we additionally verify that average bin-days per year sum up to 365.

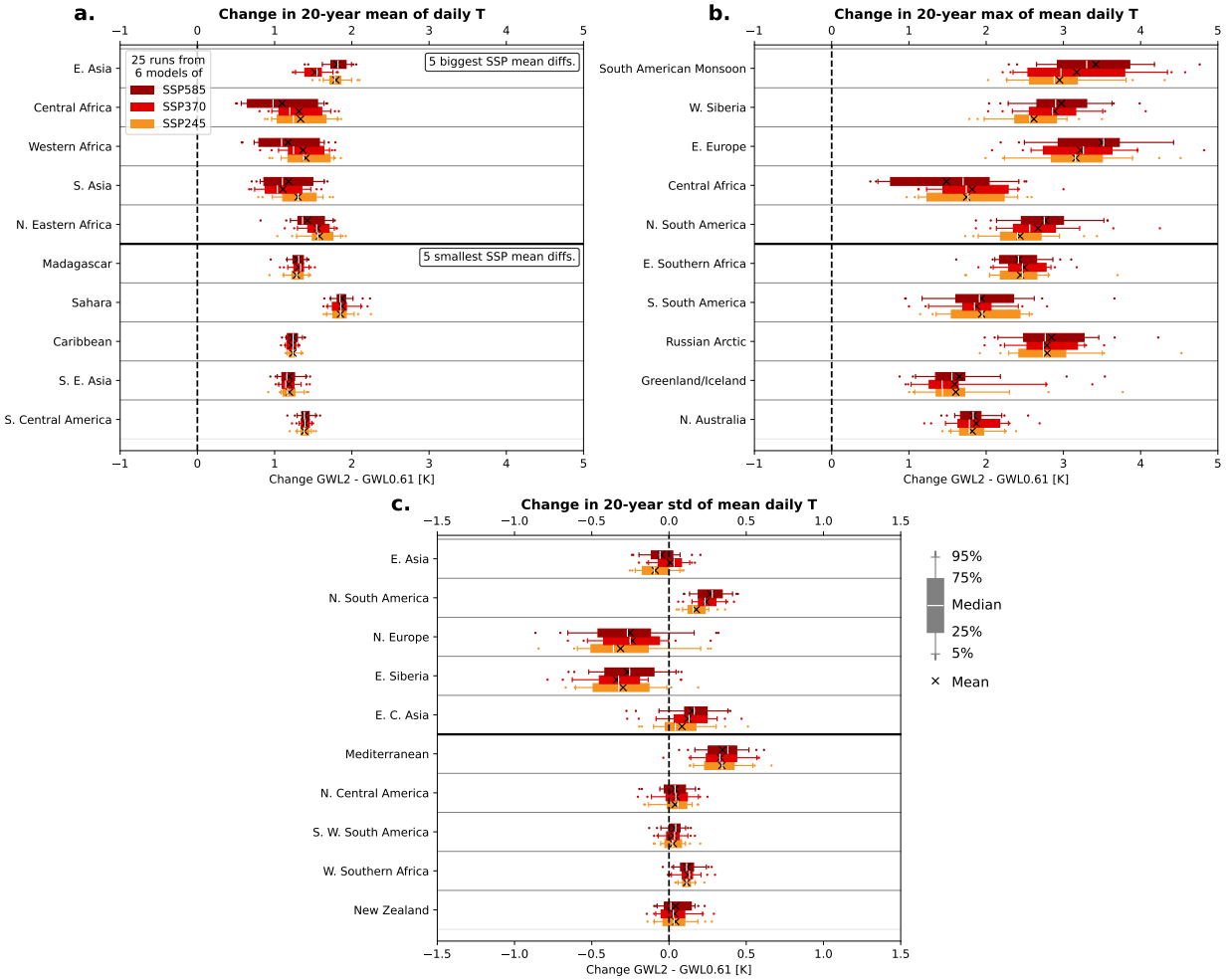

Figure 2: Changes in regionally aggregated statistics for (**a.**) mean daily temperature (**b.**) max of daily mean temperature and (**c.**) standard deviation of daily mean temperature from GWL0.61 to GWL2 by SSP. Each boxplot spans all ESMs and ensemble members. A subset of the BCD-ME is used to ensure the same number of ensemble members are in each sample to allow direct comparisons. All three panels are calculated using the 20 years surrounding each given GWL. The top half of each plot shows the 5 IPCC WG1 regions with the largest differences between SSPs at GWL2, the lower half the regions with the smallest differences.

4.3 Validation of QDM bias-correcting method

The QDM methodology uses the change in ESM temperature between GWLs and adds it to a reference bias-corrected model time series. The reference base temperature ESM series is determined using the CDF of a reanalysis dataset sampled at the quantiles of the ESM ensemble member using 31-day windows around each day-of-year to define quantiles. The CDF of this reference ESM time series should, thus, be expected to be nearly identical to the CDF of the reanalysis dataset. Differences between the two CDFs can emerge from two sources. First, we use 100 quantiles to estimate the true 621-element (31 days x 20 years) empirical CDF with quantiles between these 100 samples being linearly interpolated. Strong nonlinearities in the CDF of either the reanalysis dataset or the ESM can, thus, cause discrepancies, as can the interpolation of extremes. Second, the 30-day rolling window used to estimate quantiles could artificially narrow the resultant distributions. For example, the rolling window around the hottest day of the year is composed of that day and 30 colder days.

We test the combined influence of these factors on the differences between CDFs of the bias-corrected ESM at GWL0.61 and the corresponding reanalysis between 1982-2001. We conduct 2-sample Kolmogorov-Smirnov tests at each grid cell, using a null hypothesis that both the bias-corrected ESM and the reanalysis CDFs are drawn from the same distribution (Figure 3). Despite the high sensitivity of the Kolmogorov-Smirnov test to small differences in

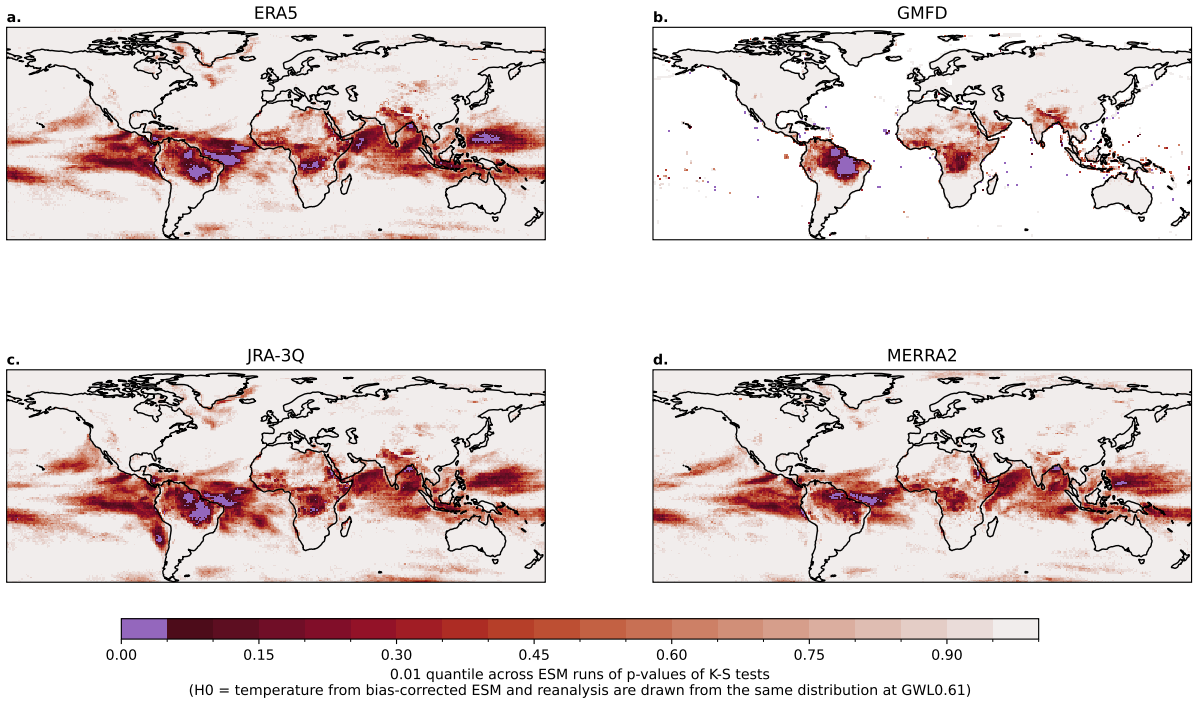

Figure 3: Maps of the 0.01 quantile across BCD-ME ensemble members of p-values of 2-sample Kolmogorov-Smirnov tests at each location against the GWL0.61 daily mean temperature distributions of each reanalysis product and each bias-corrected ensemble member of the BCD-ME being drawn from the same distribution.

CDF, low p-values are rare in our analysis. Fewer than 0.1% of grid cells in the BCD-ME ensemble member with the lowest average p-value have a p-value of less than 0.01, the benchmark significance value used in Cannon et al. (2015) (Cannon et al., 2015). These low p-values are spatially limited to locations over the tropics, particularly over the ocean.

In many of the locations with low p-values, the seasonal range of temperature is low and a 31-day rolling window captures a large fraction of the total annual temperature range. Thus, the narrowing effect of the window would be expected to be most pronounced. Correspondingly, the most anomalous bias-corrected CDFs are slightly narrower than their reanalysis counterparts (e.g. Figure 4d). However, any differences in the CDF are negligible in practice; in the location with the most differing CDFs in the ensemble member with the lowest global average p-value, the largest difference between CDFs is only 0.19 °C (Figure 4**d.**).

4.4 Comparison with NASA NEX-GDDP

To verify projected values against previously published work, we compare the BCD-ME to corresponding members of the NASA NEX-GDDP dataset (Thrasher et al., 2022) which also provides bias-corrected and downscaled daily temperature data on a near-global 0.25° grid. The datasets are not exactly comparable – NEX-GDDP provides continuous time series instead of chunks organized by GWL, the bias-correction methodologies are slightly different, and NEX-GDDP uses 1960-2014 as a reference period instead of the 20 years around GWL0.61 used in the BCD-ME. Thus, mean values of temperature are not directly comparable as 1960-2014 spans a different set of GWLs for each ESM ensemble member.

We instead compare *changes* between GWL1.5 and GWL3 for a set of ESMs, experiments, and ensemble members common to both the BCD-ME and NEX-GDDP to mitigate these differences in methods (Figure 5). To best match with NEX-GDDP, we use the the BCD-ME as bias-corrected with GMFD. We determine the GWL1.5 and GWL3 20-year periods in NEX-GDDP following our methods in Section 2.2. We expect the changes in temperature between

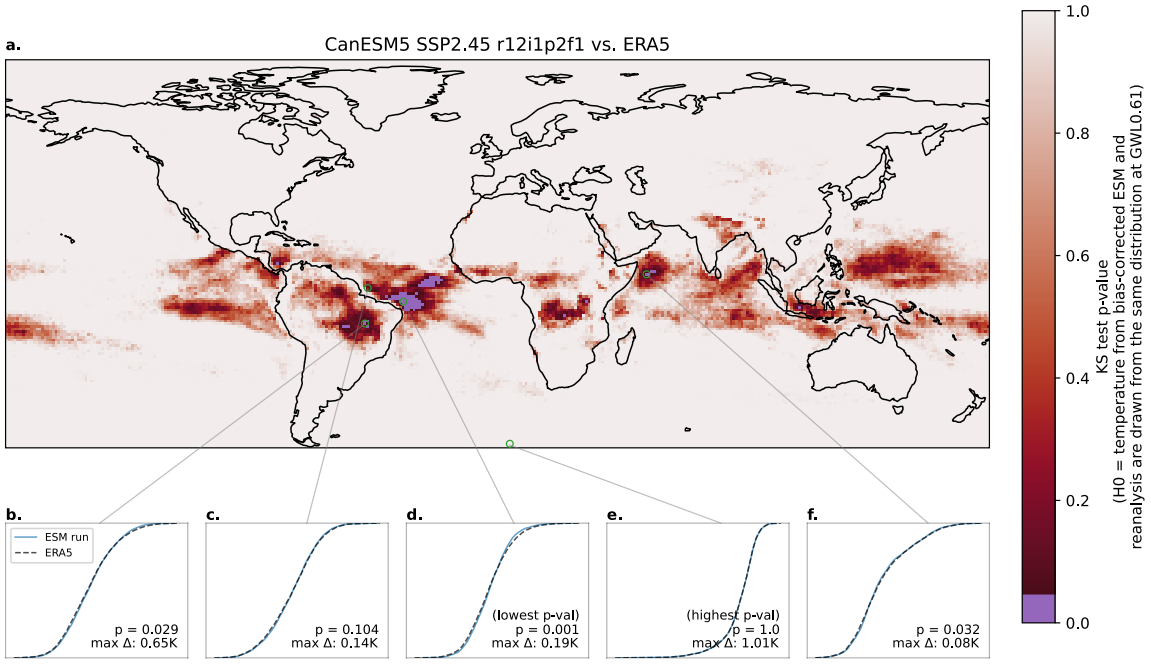

Figure 4: (**a**.) P-values of 2-sample Kolmogorov-Smirnov tests at each location comparing the ERA5 GWL0.61 daily mean temperature CDF with the CDF of a bias-corrected member from the BCD-ME. We show the r12i1p2f1 from CanESM5 run using SSP2.45, representing the BCD-ME ensemble member with the lowest average p-value, that is, the BCD-ME member for which the CDFs of the ERA5 reference distribution and the bias-corrected ESM are least similar on average. (**b**.–**f**.) CDFs of the ESM (blue line) and ERA5 (dashed black line) at various locations, including at the locations with the highest (**e**.) and lowest (**d**.) p-values. For each location, we provide the p-value and the maximum temperature difference between the two CDFs at the same quantile.

GWL1.5 and GWL3 to be similar in NEX-GDDP and the BCD-ME, though not identical, for the reasons mentioned above.

Differences between mean temperatures at each location are on the order of 0.1 °C with a global mean of about 0 in every model run tested (Figure 5). This close alignment of the two products, despite differences in methodology, provides evidence that the BCD-ME is an appropriate product for extending analyses conducted with NEX-GDDP to account for additional sources of uncertainty.

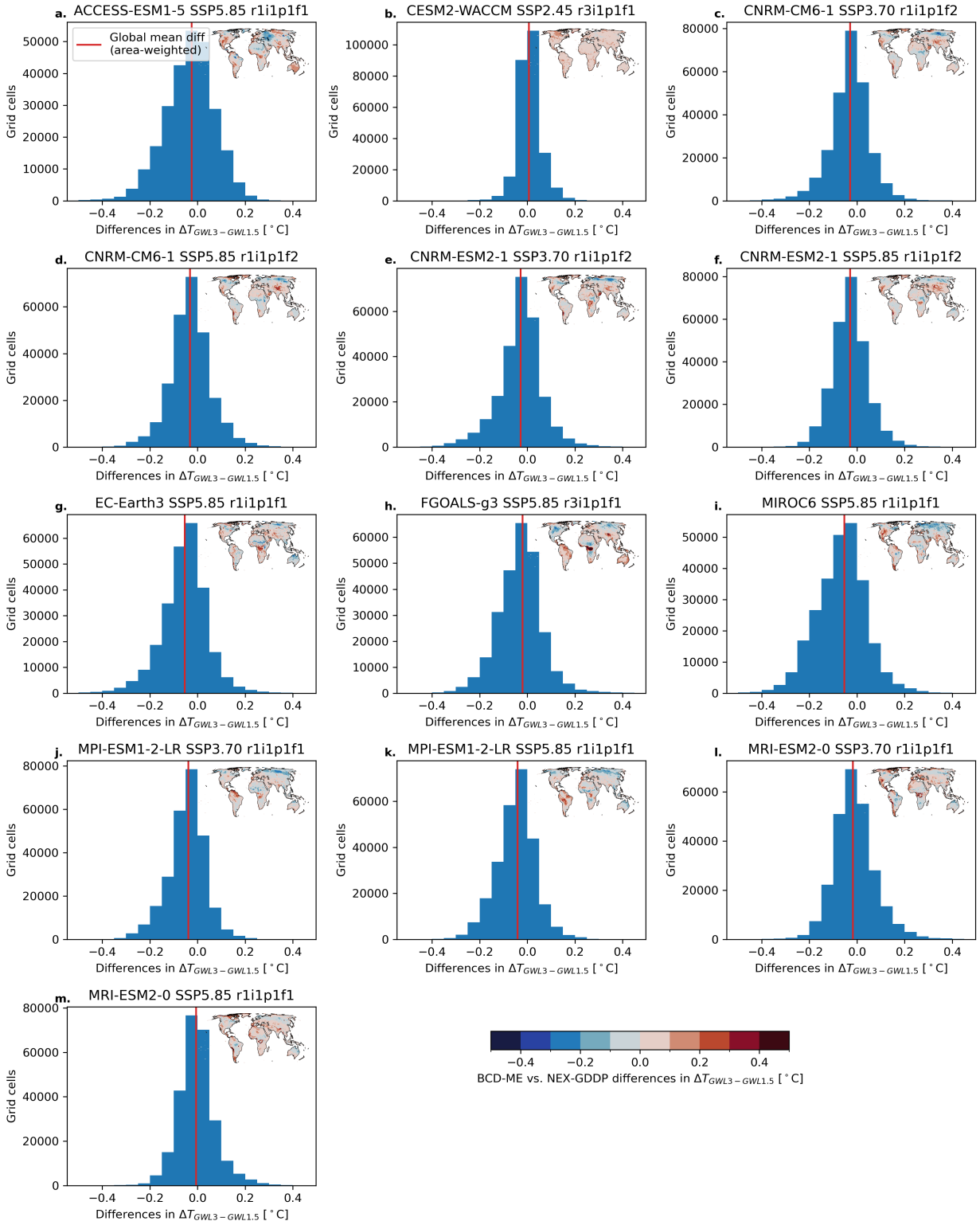

Figure 5: Histograms across grid cells of differences in mean daily temperature between changes from GWL1.5 to GWL3 between corresponding bias-corrected and downscaled ensemble members of the BCD-ME and NASA NEX-GDDP datasets. Inset maps show the spatial distribution of changes.

4.5 Uncertainty Partitioning Validation

The BCD-ME is specifically designed to test the sensitivity of climate impacts projections to three quantifiable sources of climate uncertainty: the irreducible internal variability arising from chaos in the climate system (Schwarzwald and Lenssen, 2022), the model uncertainty arising from the spread across ESMs outputs driven by the same inputs (Burke et al., 2015), and the observational uncertainty arising from differences between reanalysis estimates of the historical observed climates used to 'ground truth' projections (Casanueva et al., 2020). When a researcher utilizes the BCD-ME to propagate these climate uncertainties to their projections of temperature and related impacts, understanding if the ultimate uncertainty is primarily due to irreducible uncertainty such as internal variability, or potential reducible uncertainty such as model or observational uncertainty can guide future efforts to better constrain projections.

We thus benchmark the use of the BCD-ME for such partitioning. As such, we calculate the uncertainty partition of various changes in temperature across bias-corrected and downscaled temperature data (Figure 6). We use the Law of Total Variance to partition the total BCD-ME ensemble variance into internal variability, model uncertainty, and reanalysis uncertainty. We note that large-scale patterns of uncertainty partitioning are very similar between the bias-corrected and downscaled projections.

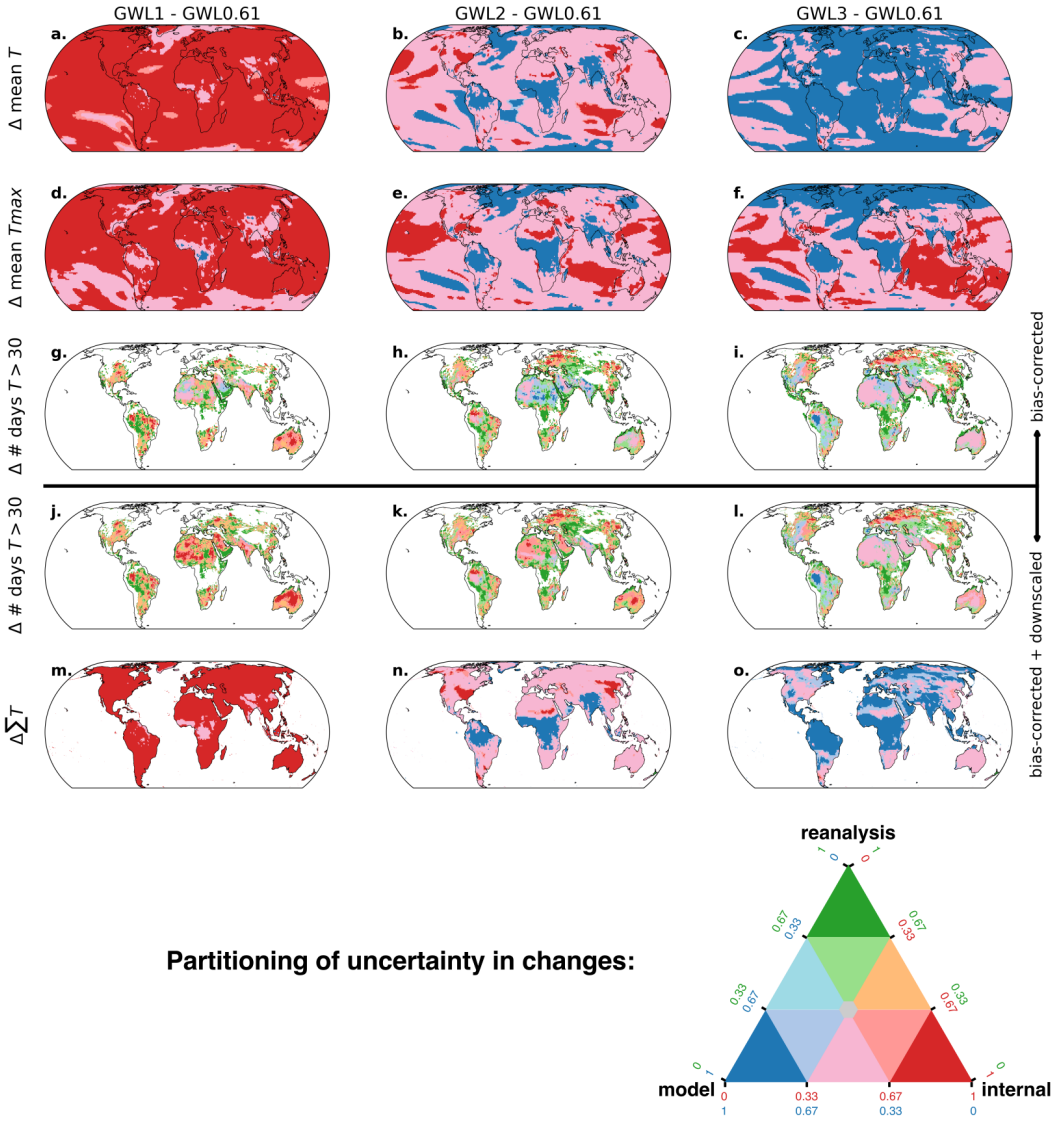

Figure 6: Sample partitioning of uncertainty using the BCD-ME for changes in mean daily temperature (panels **a.** - **c.**), maximum daily temperature (**d.** - **f.**), number of days / year with mean temperatures above 30 °C (**g.** - **l.**), and annual sum of daily temperatures (**m.** - **o.**), calculated with up to 12 runs from each ESM for each GWL. Partitioned uncertainty is shown for changes between GWL0.61 (equivalent to 1982-2001 in historical observations) and GWLs 1 (left panel), 2 (middle), and 3 (right panel). The first three rows show results for the bias-corrected set of ensembles, the last two rows show results for the bias-corrected and downscaled set of ensembles.

5 Usage Notes

The BCD-ME data structure is designed with the Python `Xarray` library and is best used in this environment. The currently plug-and-play compatibility of `Xarray` with `Zarr` for efficient and fast I/O and with `Dask` for parallel computing will provide the highest performance to software development ratio for most users. See the provided vignettes in the BCD-ME github repository for introductory examples. For context, the analysis used to create Figure 6 required 2.5 hours of computation (45 core-hours) of computation on NSF NCAR's Casper running on all 18 cores of a 2.3-GHz Intel Xeon Gold 6140 (Skylake) CPU with 10 GB RAM/core. As much of the computation is embarrassingly parallel, analysis can be expected to roughly scale with the number of CPU cores used, provided the system has sufficient I/O.

When using the BCD-ME, we recommend users cite both this study as well as the DOI of the BCD-ME data archive used to access the data. In addition, we recommend users cite the ESM simulation of any ESM used, following the citations provided in Table 4, in addition to the reanalyses used.

Model	Experiment
ACCESS-ESM1-5	SSP2-4.5 (Ziehn et al., 2019a)
	SSP5-8.5 (Ziehn et al., 2019b)
CESM2-WACCM	SSP2-4.5 (Danabasoglu, 2019a)
	SSP3-7.0 (Danabasoglu, 2019b)
	SSP5-8.5 (Danabasoglu, 2019c)
CNRM-CM6-1	SSP2-4.5 (Voldoire, 2019a)
	SSP3-7.0 (Voldoire, 2019b)
	SSP5-8.5 (Voldoire, 2019c)
CNRM-ESM2-1	SSP1-1.9 (Voldoire, 2019d)
	SSP1-2.6 (Voldoire, 2019e)
	SSP2-4.5 (Voldoire, 2019f)
	SSP3-7.0 (Voldoire, 2019g)
	SSP4-3.4 (Voldoire, 2019h)
	SSP4-6.0 (Voldoire, 2019i)
	SSP5-3.4-OS (Voldoire, 2019j)
	SSP5-8.5 (Voldoire, 2019k)
CanESM5	SSP2-4.5 (Swart et al., 2019a)
	SSP3-7.0 (Swart et al., 2019b)
	SSP5-8.5 (Swart et al., 2019c)
EC-Earth3	SSP2-4.5 (EC-Earth Consortium (EC-Earth), 2019a)
	SSP3-7.0 (EC-Earth Consortium (EC-Earth), 2019b)
	SSP5-8.5 (EC-Earth Consortium (EC-Earth), 2019c)
EC-Earth3-Veg	SSP2-4.5 (EC-Earth Consortium (EC-Earth), 2019d)
	SSP3-7.0 (EC-Earth Consortium (EC-Earth), 2019e)
	SSP5-8.5 (EC-Earth Consortium (EC-Earth), 2019f)
FGOALS-g3	SSP2-4.5 (Li, 2019a)
	SSP3-7.0 (Li, 2019b)
	SSP5-8.5 (Li, 2019c)
IPSL-CM6A-LR	SSP2-4.5 (Boucher et al., 2019a)
	SSP3-7.0 (Boucher et al., 2019b)
	SSP5-8.5 (Boucher et al., 2019c)
MIROC6	SSP2-4.5 (Shiogama et al., 2019a)
	SSP3-7.0 (Shiogama et al., 2019b)
	SSP5-8.5 (Shiogama et al., 2019c)
MPI-ESM1-2-LR	SSP2-4.5 (Wieners et al., 2019a)
	SSP3-7.0 (Wieners et al., 2019b)
	SSP5-8.5 (Wieners et al., 2019c)
MRI-ESM2-0	SSP2-4.5 (Yukimoto et al., 2019a)
	SSP3-7.0 (Yukimoto et al., 2019b)
	SSP5-8.5 (Yukimoto et al., 2019c)

Table 4: ESM citation information by ESM and scenario, following best practices for citing CMIP simulations.

6 Data Availability

The BCD-ME is freely available at `https://doi.org/10.82924/9p8f-hd64` and `https://doi.org/10.82924/k92n-qb44` under a CC-BY 4.0 license via the Earthmover Data Marketplace in Analysis-Ready, Cloud Optimized format (Abernathey et al., 2021). Users can query and interact with the with the full dataset without the need to download large files. Sample code to access this data is available as part of the replication code repository on GitHub under `https://github.com/ks905383/bcd_me/blob/main/code/sample_data_access.ipynb`.

By publication, the BCD-ME will also be hosted on the NSF NCAR GEX.

Nearly all data needed to replicate the BCD-ME processing can be downloaded entirely using the replication code below. CMIP6 ESM data was downloaded from the pangeo CMIP6 cloud database. ERA5, GMFD, and JRA-3Q data was accessed via the NCAR filesystem; this data can alternatively be downloaded directly from the publishers instead. MERRA-2 data was downloaded from the NASA GES-DISC interface.

7 Code Availability

All code required to replicate the BCD-ME and the analysis presented in this Data Descriptor is available at `https://github.com/ks905383/bcd_me/`; a final static version will be published in a frozen format along with this paper.

8 Author Contributions

Conceptualization: KS
Data Curation: KS
Formal Analysis: KS, NL
Funding Acquisition: KS, NL, RH, GW
Investigation: KS
Methodology: KS
Project Administration: KS
Resources: KS, NL
Software: KS
Supervision: KS, NL, RH, GW
Validation: KS, NL
Visualization: KS
Writing – Original Draft Preparation: NL
Writing – Review & Editing: KS, NL, RH, GW

9 Competing Interests

The authors have no known competing interests.

10 Acknowledgments

The authors thank Ryan Abernathy, Tom Bearpark, and Clara Deser for discussion that refined the BCD-ME analysis. We would like to acknowledge computing support from the Casper system (https://ncar.pub/casper) provided by the NSF National Center for Atmospheric Research (NCAR), sponsored by the National Science Foundation. We thank Adam Phillips and the NCAR Geoscience Data Exchange (GDEX) team for support with hosting the BCD-ME. We also thank Earthmover for hosting the living repository of the BCD-ME.

11 Funding

K.S. and R.H. are supported by the National Oceanic and Atmospheric Administration's Regional Integrated Sciences and Assessments Program, grant NA21OAR4310313. K.S. is also supported by the Columbia Climate School Postdoctoral Fellowship Program. N.L. is partially funded through NCAR which is sponsored by the National Science Foundation under Cooperative Agreement 1852977.

References

(2026a). BCD-ME 0.25° bias-corrected (QDM) and downscaled temperature statistics.

(2026b). BCD-ME 1° bias-corrected (QDM) temperature time series.

Abernathey, R. P., Augspurger, T., Banihirwe, A., Blackmon-Luca, C. C., Crone, T. J., Gentemann, C. L., Hamman, J. J., Henderson, N., Lepore, C., McCaie, T. A., Robinson, N. H., and Signell, R. P. (2021). Cloud-Native Repositories for Big Scientific Data. *Computing in Science & Engineering*, 23(2):26–35.

Auffhammer, M., Hsiang, S. M., Schlenker, W., and Sobel, A. (2013). Using Weather Data and Climate Model Output in Economic Analyses of Climate Change. *Review of Environmental Economics and Policy*, 7(2):181–198.

Batibeniz, F., Hauser, M., and Seneviratne, S. I. (2023). Countries most exposed to individual and concurrent extremes and near-permanent extreme conditions at different global warming levels. *Earth System Dynamics*, 14(2):485–505.

Bosilovich, M. G., Akella, S., Coy, L., Cullather, R., Draper, C., Gelaro, R., Kovach, R., Liu, Q., Molod, A., Norris, P., Wargan, K., Chao, W., Reichle, R., Takasc, L., Vikhliaev, Y., Bloom, S., Collow, A., Firth, S., Labow, G., Partyka, G., Pawson, S., Reale, O., Schubert, S. D., and Suarez, M. (2015). MERRA-2: Initial Evaluation of the Climate. Technical Report NASA/TM-2015-104606/Vol.43, NASA.

Boucher, O., Denvil, S., Levavasseur, G., Cozic, A., Caubel, A., Foujols, M.-A., Meurdesoif, Y., Cadule, P., Devilliers, M., Dupont, E., and Lurton, T. (2019a). IPSL IPSL-CM6A-LR model output prepared for CMIP6 ScenarioMIP ssp245.

Boucher, O., Denvil, S., Levavasseur, G., Cozic, A., Caubel, A., Foujols, M.-A., Meurdesoif, Y., Cadule, P., Devilliers, M., Dupont, E., and Lurton, T. (2019b). IPSL IPSL-CM6A-LR model output prepared for CMIP6 ScenarioMIP ssp370.

Boucher, O., Denvil, S., Levavasseur, G., Cozic, A., Caubel, A., Foujols, M.-A., Meurdesoif, Y., Cadule, P., Devilliers, M., Dupont, E., and Lurton, T. (2019c). IPSL IPSL-CM6A-LR model output prepared for CMIP6 ScenarioMIP ssp585.

Burke, M., Dykema, J., Lobell, D. B., Miguel, E., and Satyanath, S. (2015). Incorporating Climate Uncertainty into Estimates of Climate Change Impacts. *The Review of Economics and Statistics*, 97(2):461–471.

Cannon, A. J., Sobie, S. R., and Murdock, T. Q. (2015). Bias Correction of GCM Precipitation by Quantile Mapping: How Well Do Methods Preserve Changes in Quantiles and Extremes? *Journal of Climate*, 28(17):6938–6959.

Carleton, T., Jina, A., Delgado, M., Greenstone, M., Houser, T., Hsiang, S., Hultgren, A., Kopp, R. E., McCusker, K. E., Nath, I., Rising, J., Rode, A., Seo, H. K., Viaene, A., Yuan, J., and Zhang, A. T. (2022). Valuing the Global Mortality Consequences of Climate Change Accounting for Adaptation Costs and Benefits*. *The Quarterly Journal of Economics*, 137(4):2037–2105.

Casanueva, A., Herrera, S., Iturbide, M., Lange, S., Jury, M., Dosio, A., Maraun, D., and Gutiérrez, J. M. (2020). Testing bias adjustment methods for regional climate change applications under observational uncertainty and resolution mismatch. *Atmospheric Science Letters*, 21(7):e978.

Danabasoglu, G. (2019a). NCAR CESM2-WACCM model output prepared for CMIP6 ScenarioMIP ssp245.

Danabasoglu, G. (2019b). NCAR CESM2-WACCM model output prepared for CMIP6 ScenarioMIP ssp370.

Danabasoglu, G. (2019c). NCAR CESM2-WACCM model output prepared for CMIP6 ScenarioMIP ssp585.

Deschênes, O. and Greenstone, M. (2011). Climate Change, Mortality, and Adaptation: Evidence from Annual Fluctuations in Weather in the US. *American Economic Journal: Applied Economics*, 3(4):152–185.

EC-Earth Consortium (EC-Earth) (2019a). EC-Earth-Consortium EC-Earth3 model output prepared for CMIP6 ScenarioMIP ssp245.

EC-Earth Consortium (EC-Earth) (2019b). EC-Earth-Consortium EC-Earth3 model output prepared for CMIP6 ScenarioMIP ssp370.

EC-Earth Consortium (EC-Earth) (2019c). EC-Earth-Consortium EC-Earth3 model output prepared for CMIP6 ScenarioMIP ssp585.

EC-Earth Consortium (EC-Earth) (2019d). EC-Earth-Consortium EC-Earth3-Veg model output prepared for CMIP6 ScenarioMIP ssp245.

EC-Earth Consortium (EC-Earth) (2019e). EC-Earth-Consortium EC-Earth3-Veg model output prepared for CMIP6 ScenarioMIP ssp370.

EC-Earth Consortium (EC-Earth) (2019f). EC-Earth-Consortium EC-Earth3-Veg model output prepared for CMIP6 ScenarioMIP ssp585.

Eyring, V., Bony, S., Meehl, G. A., Senior, C. A., Stevens, B., Stouffer, R. J., and Taylor, K. E. (2016). Overview of the Coupled Model Intercomparison Project Phase 6 (CMIP6) experimental design and organization. *Geoscientific Model Development*, 9(5):1937–1958.

Frieler, K., Volkholz, J., Lange, S., Schewe, J., Mengel, M., Del Rocío Rivas López, M., Otto, C., Reyer, C. P. O., Karger, D. N., Malle, J. T., Treu, S., Menz, C., Blanchard, J. L., Harrison, C. S., Petrik, C. M., Eddy, T. D., Ortega-Cisneros, K., Novaglio, C., Rousseau, Y., Watson, R. A., Stock, C., Liu, X., Heneghan, R., Tittensor, D., Maury, O., Büchner, M., Vogt, T., Wang, T., Sun, F., Sauer, I. J., Koch, J., Vanderkelen, I., Jägermeyr, J., Müller, C., Rabin, S., Klar, J., Vega Del Valle, I. D., Lasslop, G., Chadburn, S., Burke, E., Gallego-Sala, A., Smith, N., Chang, J., Hantson, S., Burton, C., Gädeke, A., Li, F., Gosling, S. N., Müller Schmied, H., Hattermann, F., Wang, J., Yao, F., Hickler, T., Marcé, R., Pierson, D., Thiery, W., Mercado-Bettín, D., Ladwig, R., Ayala-Zamora, A. I., Forrest, M., and Bechtold, M. (2024). Scenario setup and forcing data for impact model evaluation and impact attribution within the third round of the Inter-Sectoral Impact Model Intercomparison Project (ISIMIP3a). *Geoscientific Model Development*, 17(1):1–51.

Gelaro, R., McCarty, W., Suárez, M. J., Todling, R., Molod, A., Takacs, L., Randles, C. A., Darmenov, A., Bosilovich, M. G., Reichle, R., Wargan, K., Coy, L., Cullather, R., Draper, C., Akella, S., Buchard, V., Conaty, A., Da Silva, A. M., Gu, W., Kim, G.-K., Koster, R., Lucchesi, R., Merkova, D., Nielsen, J. E., Partyka, G., Pawson, S., Putman, W., Rienecker, M., Schubert, S. D., Sienkiewicz, M., and Zhao, B. (2017). The Modern-Era Retrospective Analysis for Research and Applications, Version 2 (MERRA-2). *Journal of Climate*, 30(14):5419–5454.

Gergel, D. R., Malevich, S. B., McCusker, K. E., Tenezakis, E., Delgado, M. T., Fish, M. A., and Kopp, R. E. (2024). Global Downscaled Projections for Climate Impacts Research (GDPCIR): Preserving quantile trends for modeling future climate impacts. *Geoscientific Model Development*, 17(1):191–227.

Hartke, S. H., Newman, A. J., Gutmann, E., McCrary, R., Lybarger, N. D., and Lehner, F. (2024). GARD-LENS: A downscaled large ensemble dataset for understanding future climate and its uncertainties. *Scientific Data*, 11(1):1374.

Hausfather, Z., Marvel, K., Schmidt, G. A., Nielsen-Gammon, J. W., and Zelinka, M. (2022). Climate simulations: Recognize the 'hot model' problem. *Nature*, 605(7908):26–29.

Hawkins, E. and Sutton, R. (2009). The Potential to Narrow Uncertainty in Regional Climate Predictions. *Bulletin of the American Meteorological Society*, 90(8):1095–1108.

Hersbach, H., Bell, B., Berrisford, P., Hirahara, S., Horányi, A., Muñoz-Sabater, J., Nicolas, J., Peubey, C., Radu, R., Schepers, D., Simmons, A., Soci, C., Abdalla, S., Abellan, X., Balsamo, G., Bechtold, P., Biavati, G., Bidlot, J., Bonavita, M., De Chiara, G., Dahlgren, P., Dee, D., Diamantakis, M., Dragani, R., Flemming, J., Forbes, R., Fuentes, M., Geer, A., Haimberger, L., Healy, S., Hogan, R. J., Hólm, E., Janisková, M., Keeley, S., Laloyaux, P., Lopez, P., Lupu, C., Radnoti, G., De Rosnay, P., Rozum, I., Vamborg, F., Villaume, S., and Thépaut, J.-N. (2020). The ERA5 global reanalysis. *Quarterly Journal of the Royal Meteorological Society*, 146(730):1999–2049.

Hsiang, S., Kopp, R., Jina, A., Rising, J., Delgado, M., Mohan, S., Rasmussen, D. J., Muir-Wood, R., Wilson, P., Oppenheimer, M., Larsen, K., and Houser, T. (2017). Estimating economic damage from climate change in the United States. *Science*, 356(6345):1362–1369.

Hultgren, A., Carleton, T., Delgado, M., Gergel, D. R., Greenstone, M., Houser, T., Hsiang, S., Jina, A., Kopp, R. E., Malevich, S. B., McCusker, K. E., Mayer, T., Nath, I., Rising, J., Rode, A., and Yuan, J. (2025). Impacts of climate change on global agriculture accounting for adaptation. *Nature*, 642(8068):644–652.

Kosaka, Y., Kobayashi, S., Harada, Y., Kobayashi, C., Naoe, H., Yoshimoto, K., Harada, M., Goto, N., Chiba, J., Miyaoka, K., Sekiguchi, R., Deushi, M., Kamahori, H., Nakaegawa, T., Tanaka, T. Y., Tokuhiro, T., Sato, Y., Matsushita, Y., and Onogi, K. (2024). The JRA-3Q Reanalysis. *Journal of the Meteorological Society of Japan. Ser. II*, 102(1):49–109.

Lenssen, N., Schmidt, G. A., Hendrickson, M., Jacobs, P., Menne, M. J., and Ruedy, R. (2024). A NASA GISTEMPv4 Observational Uncertainty Ensemble. *Journal of Geophysical Research: Atmospheres*, 129(17):e2023JD040179.

Li, L. (2019a). CAS FGOALS-g3 model output prepared for CMIP6 ScenarioMIP ssp245.

Li, L. (2019b). CAS FGOALS-g3 model output prepared for CMIP6 ScenarioMIP ssp370.

Li, L. (2019c). CAS FGOALS-g3 model output prepared for CMIP6 ScenarioMIP ssp585.

Maraun, D. (2016). Bias Correcting Climate Change Simulations - a Critical Review. *Current Climate Change Reports*, 2(4):211–220.

Milinski, S., Maher, N., and Olonscheck, D. (2020). How large does a large ensemble need to be? *Earth System Dynamics*, 11(4):885–901.

Morice, C. P., Kennedy, J. J., Rayner, N. A., Winn, J. P., Hogan, E., Killick, R. E., Dunn, R. J. H., Osborn, T. J., Jones, P. D., and Simpson, I. R. (2021). An Updated Assessment of Near-Surface Temperature Change From 1850: The HadCRUT5 Data Set. *Journal of Geophysical Research: Atmospheres*, 126(3):e2019JD032361.

Pierce, D. W., Cayan, D. R., Feldman, D. R., and Risser, M. D. (2023). Future Increases in North American Extreme Precipitation in CMIP6 Downscaled with LOCA. *Journal of Hydrometeorology*, 24(5):951–975.

Riahi, K., van Vuuren, D. P., Kriegler, E., Edmonds, J., O'Neill, B. C., Fujimori, S., Bauer, N., Calvin, K., Dellink, R., Fricko, O., Lutz, W., Popp, A., Cuaresma, J. C., Kc, S., Leimbach, M., Jiang, L., Kram, T., Rao, S., Emmerling, J., Ebi, K., Hasegawa, T., Havlik, P., Humpenöder, F., Da Silva, L. A., Smith, S., Stehfest, E., Bosetti, V., Eom, J., Gernaat, D., Masui, T., Rogelj, J., Strefler, J., Drouet, L., Krey, V., Luderer, G., Harmsen, M., Takahashi, K., Baumstark, L., Doelman, J. C., Kainuma, M., Klimont, Z., Marangoni, G., Lotze-Campen, H., Obersteiner, M., Tabeau, A., and Tavoni, M. (2017). The Shared Socioeconomic Pathways and their energy, land use, and greenhouse gas emissions implications: An overview. *Global Environmental Change*, 42:153–168.

Rising, J., Tedesco, M., Piontek, F., and Stainforth, D. A. (2022). The missing risks of climate change. *Nature*, 610(7933):643–651.

Rode, A., Carleton, T., Delgado, M., Greenstone, M., Houser, T., Hsiang, S., Hultgren, A., Jina, A., Kopp, R. E., McCusker, K. E., Nath, I., Rising, J., and Yuan, J. (2021). Estimating a social cost of carbon for global energy consumption. *Nature*, 598(7880):308–314.

Schlenker, W. and Roberts, M. J. (2009). Nonlinear temperature effects indicate severe damages to U.S. crop yields under climate change. *Proceedings of the National Academy of Sciences*, 106(37):15594–15598.

Schulze, R. (2000). Transcending scales of space and time in impact studies of climate and climate change on agrohydrological responses. *Agriculture, Ecosystems & Environment*, 82(1-3):185–212.

Schwarzwald, K. and Lenssen, N. (2022). The importance of internal climate variability in climate impact projections. *Proceedings of the National Academy of Sciences*, 119(42):e2208095119.

Seneviratne, S. I. and Hauser, M. (2020). Regional Climate Sensitivity of Climate Extremes in CMIP6 Versus CMIP5 Multimodel Ensembles. *Earth's Future*, 8(9):e2019EF001474.

Sheffield, J., Goteti, G., and Wood, E. F. (2006). Development of a 50-Year High-Resolution Global Dataset of Meteorological Forcings for Land Surface Modeling. *Journal of Climate*, 19(13):3088–3111.

Shiogama, H., Abe, M., and Tatebe, H. (2019a). MIROC MIROC6 model output prepared for CMIP6 ScenarioMIP ssp245.

Shiogama, H., Abe, M., and Tatebe, H. (2019b). MIROC MIROC6 model output prepared for CMIP6 ScenarioMIP ssp370.

Shiogama, H., Abe, M., and Tatebe, H. (2019c). MIROC MIROC6 model output prepared for CMIP6 ScenarioMIP ssp585.

Shiogama, H., Fujimori, S., Hasegawa, T., Hayashi, M., Hirabayashi, Y., Ogura, T., Iizumi, T., Takahashi, K., and Takemura, T. (2023). Important distinctiveness of SSP3–7.0 for use in impact assessments. *Nature Climate Change*, 13(12):1276–1278.

Swart, N. C., Cole, J. N., Kharin, V. V., Lazare, M., Scinocca, J. F., Gillett, N. P., Anstey, J., Arora, V., Christian, J. R., Jiao, Y., Lee, W. G., Majaess, F., Saenko, O. A., Seiler, C., Seinen, C., Shao, A., Solheim, L., von Salzen, K., Yang, D., Winter, B., and Sigmond, M. (2019a). CCCma CanESM5 model output prepared for CMIP6 ScenarioMIP ssp245.

Swart, N. C., Cole, J. N., Kharin, V. V., Lazare, M., Scinocca, J. F., Gillett, N. P., Anstey, J., Arora, V., Christian, J. R., Jiao, Y., Lee, W. G., Majaess, F., Saenko, O. A., Seiler, C., Seinen, C., Shao, A., Solheim, L., von Salzen, K., Yang, D., Winter, B., and Sigmond, M. (2019b). CCCma CanESM5 model output prepared for CMIP6 ScenarioMIP ssp370.

Swart, N. C., Cole, J. N., Kharin, V. V., Lazare, M., Scinocca, J. F., Gillett, N. P., Anstey, J., Arora, V., Christian, J. R., Jiao, Y., Lee, W. G., Majaess, F., Saenko, O. A., Seiler, C., Seinen, C., Shao, A., Solheim, L., von Salzen, K., Yang, D., Winter, B., and Sigmond, M. (2019c). CCCma CanESM5 model output prepared for CMIP6 ScenarioMIP ssp585.

Tebaldi, C. and Knutti, R. (2007). The use of the multi-model ensemble in probabilistic climate projections. *Philosophical Transactions of the Royal Society A: Mathematical, Physical and Engineering Sciences*, 365(1857):2053–2075.

Thrasher, B., Wang, W., Michaelis, A., Melton, F., Lee, T., and Nemani, R. (2022). NASA Global Daily Downscaled Projections, CMIP6. *Scientific Data*, 9(1):262.

Voldoire, A. (2019a). CNRM-CERFACS CNRM-CM6-1 model output prepared for CMIP6 ScenarioMIP ssp245.

Voldoire, A. (2019b). CNRM-CERFACS CNRM-CM6-1 model output prepared for CMIP6 ScenarioMIP ssp370.

Voldoire, A. (2019c). CNRM-CERFACS CNRM-CM6-1 model output prepared for CMIP6 ScenarioMIP ssp585.

Voldoire, A. (2019d). CNRM-CERFACS CNRM-ESM2-1 model output prepared for CMIP6 ScenarioMIP ssp119.

Voldoire, A. (2019e). CNRM-CERFACS CNRM-ESM2-1 model output prepared for CMIP6 ScenarioMIP ssp126.

Voldoire, A. (2019f). CNRM-CERFACS CNRM-ESM2-1 model output prepared for CMIP6 ScenarioMIP ssp245.

Voldoire, A. (2019g). CNRM-CERFACS CNRM-ESM2-1 model output prepared for CMIP6 ScenarioMIP ssp370.

Voldoire, A. (2019h). CNRM-CERFACS CNRM-ESM2-1 model output prepared for CMIP6 ScenarioMIP ssp434.

Voldoire, A. (2019i). CNRM-CERFACS CNRM-ESM2-1 model output prepared for CMIP6 ScenarioMIP ssp460.

Voldoire, A. (2019j). CNRM-CERFACS CNRM-ESM2-1 model output prepared for CMIP6 ScenarioMIP ssp534-over.

Voldoire, A. (2019k). CNRM-CERFACS CNRM-ESM2-1 model output prepared for CMIP6 ScenarioMIP ssp585.

Wieners, K.-H., Giorgetta, M., Jungclaus, J., Reick, C., Esch, M., Bittner, M., Gayler, V., Haak, H., de Vrese, P., Raddatz, T., Mauritsen, T., von Storch, J.-S., Behrens, J., Brovkin, V., Claussen, M., Crueger, T., Fast, I., Fiedler, S., Hagemann, S., Hohenegger, C., Jahns, T., Kloster, S., Kinne, S., Lasslop, G., Kornblueh, L., Marotzke, J., Matei, D., Meraner, K., Mikolajewicz, U., Modali, K., Müller, W., Nabel, J., Notz, D., Peters-von Gehlen, K., Pincus, R., Pohlmann, H., Pongratz, J., Rast, S., Schmidt, H., Schnur, R., Schulzweida, U., Six, K., Stevens, B., Voigt, A., and Roeckner, E. (2019a). MPI-M MPI-ESM1.2-LR model output prepared for CMIP6 ScenarioMIP ssp245.

Wieners, K.-H., Giorgetta, M., Jungclaus, J., Reick, C., Esch, M., Bittner, M., Gayler, V., Haak, H., de Vrese, P., Raddatz, T., Mauritsen, T., von Storch, J.-S., Behrens, J., Brovkin, V., Claussen, M., Crueger, T., Fast, I., Fiedler, S., Hagemann, S., Hohenegger, C., Jahns, T., Kloster, S., Kinne, S., Lasslop, G., Kornblueh, L., Marotzke, J., Matei, D., Meraner, K., Mikolajewicz, U., Modali, K., Müller, W., Nabel, J., Notz, D., Peters-von Gehlen, K., Pincus, R., Pohlmann, H., Pongratz, J., Rast, S., Schmidt, H., Schnur, R., Schulzweida, U., Six, K., Stevens, B., Voigt, A., and Roeckner, E. (2019b). MPI-M MPI-ESM1.2-LR model output prepared for CMIP6 ScenarioMIP ssp370.

Wieners, K.-H., Giorgetta, M., Jungclaus, J., Reick, C., Esch, M., Bittner, M., Gayler, V., Haak, H., de Vrese, P., Raddatz, T., Mauritsen, T., von Storch, J.-S., Behrens, J., Brovkin, V., Claussen, M., Crueger, T., Fast, I., Fiedler, S., Hagemann, S., Hohenegger, C., Jahns, T., Kloster, S., Kinne, S., Lasslop, G., Kornblueh, L., Marotzke, J., Matei, D., Meraner, K., Mikolajewicz, U., Modali, K., Müller, W., Nabel, J., Notz, D., Peters-von Gehlen, K., Pincus, R., Pohlmann, H., Pongratz, J., Rast, S., Schmidt, H., Schnur, R., Schulzweida, U., Six, K., Stevens, B., Voigt, A., and Roeckner, E. (2019c). MPI-M MPI-ESM1.2-LR model output prepared for CMIP6 ScenarioMIP ssp585.

Yukimoto, S., Koshiro, T., Kawai, H., Oshima, N., Yoshida, K., Urakawa, S., Tsujino, H., Deushi, M., Tanaka, T., Hosaka, M., Yoshimura, H., Shindo, E., Mizuta, R., Ishii, M., Obata, A., and Adachi, Y. (2019a). MRI MRI-ESM2.0 model output prepared for CMIP6 ScenarioMIP ssp245.

Yukimoto, S., Koshiro, T., Kawai, H., Oshima, N., Yoshida, K., Urakawa, S., Tsujino, H., Deushi, M., Tanaka, T., Hosaka, M., Yoshimura, H., Shindo, E., Mizuta, R., Ishii, M., Obata, A., and Adachi, Y. (2019b). MRI MRI-ESM2.0 model output prepared for CMIP6 ScenarioMIP ssp370.

Yukimoto, S., Koshiro, T., Kawai, H., Oshima, N., Yoshida, K., Urakawa, S., Tsujino, H., Deushi, M., Tanaka, T., Hosaka, M., Yoshimura, H., Shindo, E., Mizuta, R., Ishii, M., Obata, A., and Adachi, Y. (2019c). MRI MRI-ESM2.0 model output prepared for CMIP6 ScenarioMIP ssp585.

Ziehn, T., Chamberlain, M., Lenton, A., Law, R., Bodman, R., Dix, M., Wang, Y., Dobrohotoff, P., Srbinovsky, J., Stevens, L., Vohralik, P., Mackallah, C., Sullivan, A., O'Farrell, S., and Druken, K. (2019a). CSIRO ACCESS-ESM1.5 model output prepared for CMIP6 ScenarioMIP ssp245.

Ziehn, T., Chamberlain, M., Lenton, A., Law, R., Bodman, R., Dix, M., Wang, Y., Dobrohotoff, P., Srbinovsky, J., Stevens, L., Vohralik, P., Mackallah, C., Sullivan, A., O'Farrell, S., and Druken, K. (2019b). CSIRO ACCESS-ESM1.5 model output prepared for CMIP6 ScenarioMIP ssp585.